2015 International Symposium on Nonlinear Theory and its Applications
NOLTA2015, Kowloon, Hong Kong, China, December 1-4, 2015

Resonant converter designs applying computation algorithms of bifurcation values

Y. Yamada†, T. Nagashima† and H. Sekiya†

†Graduate School of Advanced Integration Science, Chiba University 1-33,
Yayoi-cho, Inage-ku, Chiba, 263-8522 JAPAN.
Email: yt.yamada@chiba-u.jp, sekiya@faculty.chiba-u.jp

Abstract—This paper proposes a design method of resonant converters applying computation algorithm of bifurcation values. As a design example, the phase-controlled resonant dc-dc converter with the class-D Zero-Voltage Switching (ZVS) inverter and the class-E rectifier is designed. By drawing the ZVS region on the parameter space, it is possible to obtain the proper component values for satisfying the ZVS condition at any phase shifts. The validity of the design method was confirmed from the quantitative agreements with PSpice-simulation and experimental results.

1. Introduction

Resonant converters are widely used as power-electronics circuits for RF power supply [1], wireless power transfer system [2] and so on. One of the design motivations of the resonant converters and inverters is an achievement of the soft switching conditions such as Zero-Voltage Switching (ZVS) condition.

The phase control [3] is a major control strategy to achieve the soft switching in the wide control-parameter region. By changing the phase shift between two inverters, the amplitude of the sinusoidal current can be adjusted and output-power control is achieved. It is, however, not simple to design the phase-controlled converter for achieving ZVS at any phase shifts. This is because the ZVS condition is sensitive to load variations. Therefore, it is important to comprehend the switching states in wide parameter region for determining proper system parameters.

By the way, switching converters are regarded as typical nonlinear systems with periodic external forces. Therefore, the power-electronics research field is very familiar with nonlinear-system analysis research field. In the nonlinear research field, there is the special computation algorithm for obtaining bifurcation values [4]. The bifurcation-value derivation problem narrows down to the derivation of the system parameters, which satisfy the bifurcation and steady-state conditions simultaneously. On the other hand, most of power-electronics-circuit characteristics such as switching conditions and output power are defined in the steady state. Namely, it is possible to derive system parameters of the power-electronics circuits for satisfying the assigned design conditions with high accuracy and low computation cost when the computation algorithm of bifurcation values is applied to the circuit designs.

This paper presents a design method of resonant converter applying computation algorithm of bifurcation values. As a design example, the phase-controlled resonant dc-dc converter with the class-D ZVS inverter and the class-E rectifier is designed. By drawing the ZVS region on the parameter space, it is possible to obtain the proper component values for satisfying the ZVS condition at any phase shifts. The validity of the design method was confirmed from the quantitative agreements with PSpice-simulation and experimental results. The maximum efficiency of the designed converter is 95.8% with 400 kHz operation and 50 W output power.

2. Summary of Design Algorithm

The computation algorithm for bifurcation-value derivations has special computation techniques, which provides rigorous bifurcation values with low computation cost regardless of the system complexity. In this paper, computation algorithm in [4] is basis for the proposed algorithm.

2.1. System Description

Let us consider a dynamical system described by differential equations:

$$\frac{d\boldsymbol{x}}{dt} = f(t, \boldsymbol{x}, \boldsymbol{\lambda}), \tag{1}$$

where $t \in \boldsymbol{R}$, $\boldsymbol{x} \in \boldsymbol{R}^n$, and $\boldsymbol{\lambda} \in \boldsymbol{R}^m$ denote time, n-dimensional state, and m-dimensional system parameter, respectively. In this paper, for sake of simplicity,

$$\begin{array}{rcl} f : \boldsymbol{R} \times \boldsymbol{R}^n \times \boldsymbol{R}^m & \rightarrow & \boldsymbol{R}^n \\ (t, \boldsymbol{x}, \boldsymbol{\lambda}) & \mapsto & f(t, \boldsymbol{x}, \boldsymbol{\lambda}) \end{array} \tag{2}$$

is periodic function in t with period t_T :

$$f(t + t_T, \boldsymbol{x}, \boldsymbol{\lambda}) = f(t, \boldsymbol{x}, \boldsymbol{\lambda}). \tag{3}$$

We also assume that (1) has a solution $\boldsymbol{x}(t) = \boldsymbol{\varphi}(t, \boldsymbol{x_0}, \boldsymbol{\lambda})$ defined on $-\infty < t < \infty$ with every initial condition $\boldsymbol{x_0} \in \boldsymbol{R}^n$ and every $\boldsymbol{\lambda} \in \boldsymbol{R}^m$: $\boldsymbol{x}(0) = \boldsymbol{\varphi}(0, \boldsymbol{x_0}, \boldsymbol{\lambda}) = \boldsymbol{x_0}$.

2.2. Poincaré Mapping and Steady-State Conditions

By the periodic hypothesis (3), it is natural to define a C^∞ diffeomorphism T from state space $\boldsymbol{R}^n$ into itself :

$$\begin{array}{rcl} T : \boldsymbol{R}^n & \rightarrow & \boldsymbol{R}^n \\ \boldsymbol{x_0} & \mapsto & T(\boldsymbol{x_0}, \boldsymbol{\lambda}) = \boldsymbol{\varphi}(t_T, \boldsymbol{x_0}, \boldsymbol{\lambda}). \end{array} \tag{4}$$

The mapping T is often called the Poincaré mapping and is used for investigating qualitative properties of (1).

If a solution $\boldsymbol{x}(t) = \boldsymbol{\varphi}(t, \boldsymbol{p_0}, \boldsymbol{\lambda})$ is periodic with period t_T, the point $\boldsymbol{p_0} \in \boldsymbol{R}^n$ is a fixed point of T :

$$T(\ \boldsymbol{p_0}\ , \boldsymbol{\lambda}\ ) = \boldsymbol{p_0}. \tag{5}$$

If $\boldsymbol{p_0} = \boldsymbol{x_0}$, (5) corresponds to the boundary conditions for the steady state. The initial values $\boldsymbol{x_0}$ for the steady state can be determined uniquely by solving (5) with $\boldsymbol{p_0} = \boldsymbol{x_0}$.

2.3. Power-Electronics Circuit Design Conditions

Power electronics circuits such as switching converters can be expressed by differential equations with periodic external forces as given in (1). Additionally, most of design restrictions of the switching converters are evaluated in the steady state. Because it is necessary to consider multiple conditions for the circuit designs, we have

$$G(\boldsymbol{x_0}, \boldsymbol{\lambda}) = \begin{bmatrix} G_1(\boldsymbol{x_0}, \boldsymbol{\lambda}) \\ G_2(\boldsymbol{x_0}, \boldsymbol{\lambda}) \\ \vdots \\ G_N(\boldsymbol{x_0}, \boldsymbol{\lambda}) \end{bmatrix} = \boldsymbol{O}. \quad (6)$$

When (5) and (6) are solved simultaneously by using Newton's method, it can be obtained $\boldsymbol{x_0}$ for guaranteeing the steady-state conditions and $\boldsymbol{\lambda}$ for achieving the design conditions simultaneously.

2.4. Boundary-Curve Tracking

The visualization of system characteristics in two-dimensional parameter space (λ_1, λ_2) is considered. When characteristics are investigated all the sampling points of parameter space, high computation cost is necessary for the characteristic comprehensions. The characteristics can be visualized with low computation cost by drawing the boundary curves, which is our proposal for the computation-cost problem. (λ_{1l}, λ_{2l}) expresses the lth parameter set for satisfying the assigned conditions and subscription l means the number of iteration. It is assumed that the first parameter set (λ_{10}, λ_{20}) for satisfying the assigned conditions can be obtained. For boundary curve derivations, one of the parameters is slightly changed, e.g., $\lambda_{11} = \lambda_{10} + \varepsilon_{\lambda_1}$, where ε_{λ_m} is a sampling interval on the parameter space for λ_m. The other parameter, namely λ_{21} can be determined from the parameter-derivation algorithm. By changing the system parameter slightly, Newton's method is converged with a few iterations.

It is necessary to know the direction and the slope for following the boundary curve. The direction and slope can be obtained approximately from

$$(\Delta_{\lambda_{1l}}, \Delta_{\lambda_{2l}}) = [(\lambda_{1l} - \lambda_{1(l-1)})/\varepsilon_{\lambda_1}, (\lambda_{2l} - \lambda_{2(l-1)})/\varepsilon_{\lambda_2}]. \quad (7)$$

By using (7), the parameter for obtaining the l+1th solution is renewed as

$$\begin{cases} \lambda_{1(l+1)} = \lambda_{1l} + (-1)\mathrm{sgn}(\Delta_{\lambda_{1l}})\varepsilon_{\lambda_1} & \text{if } \Delta_{\lambda_{1l}} > \Delta_{\lambda_{2l}}, \\ \lambda_{2(l+1)} = \lambda_{2l} + (-1)\mathrm{sgn}(\Delta_{\lambda_{2l}})\varepsilon_{\lambda_2} & \text{if } \Delta_{\lambda_{2l}} > \Delta_{\lambda_{1l}}. \end{cases} \quad (8)$$

When the above computations are iterated against l, the boundary curve can be followed automatically in the parameter space.

3. Design Example

3.1. Phase-Controlled Class-D Inverter

The phase-controlled class-D inverter is composed of two identical class-D inverters, which are connected in parallel. Each inverter consists of input voltage source V_I, two MOSFETs as switching devices S_{1j} and S_{2j}, shunt capacitances C_{S1j} and C_{S2j}, and series-resonant circuit $L_{rj} - C_{rj}$, where the subscript j is a label of the inverters. The top and bottom switches at each inverter turns on and off alternatively with the switch on-duty ratio D, where $D < 0.5$ for generating the dead time. The ac current i_{rj} is generated by the series-resonant filter $L_{rj} - C_{rj}$. The rectifier input current i, where $i = i_{r1} + i_{r2}$, is fed into the class-E rectifier. The amplitude of i can be controlled by the phase shift between the inverters ϕ, which means that the output power can be adjusted by changing the phase shift. A maximum and minimum rectifier input currents are yielded at $\phi = 0$ and $\phi = \pi$, respectively.

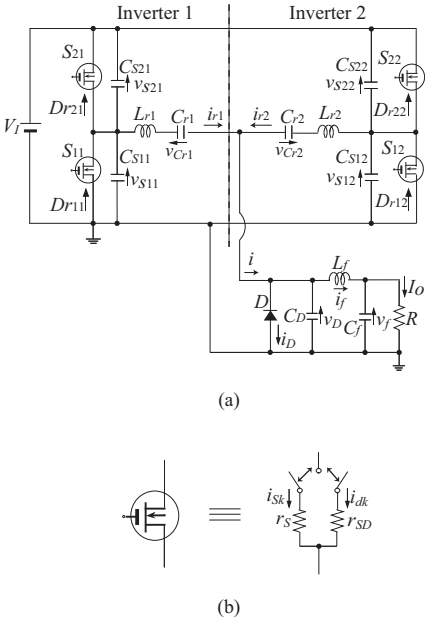

Figure 1: Phase-controlled resonant dc-dc converter with the class-D ZVS inverter and the class-E rectifier. (a) Circuit topology. (b) Equivalent switching device model.

3.2. Class-E Rectifier

The class-E rectifier consists of diode D, diode-shunt capacitance C_D, low-pass filter $L_f - C_f$, and load resistance R as shown in Figure 1. In the class-E rectifier, the difference of the input current i and the output current I_o flows through the diode D or the shunt capacitance C_D alternatively. During the diode is in off state, the current flows through the shunt capacitance. The diode voltage is transformed into a DC voltage through the $L_f - C_f$ low-pass filter. In the diode-on duration, the diode voltage v_D is approximately zero, which leads to the ZVS at turn-off instant. At the turn-off transition of the diode, diode voltage and the slope of it are zero, which are called class-E ZVS/ZDS conditions. Because of the class-E ZVS/ZDS conditions, the class-E rectifier can also achieve high power-conversion efficiency. It is noted that the class-E rectifier always achieves the class-E ZVS/ZDS conditions regardless of the circuit parameters, which is different from the class-D ZVS inverter.

The phase-controlled resonant converter as shown in Fig. 1 can achieve a high power-conversion efficiency when the phase-controlled inverter satisfies the ZVS condition. Therefore, it is quite important to ensure that the phase-controlled inverter achieves the ZVS at any phase shifts.

3.3. Circuit Description

The following assumptions are given for converter modeling.

1) All the switching devices, which are MOSFETs, MOSFET anti-parallel diodes, and rectifier diode

work as ideal switching devices; namely zero switching time and infinite off-resistance are assumed.

2) The switch-on resistance of MOSFETs, anti-parallel diodes, and rectifier diode are considered, which are expressed as r_S, r_{SD}, and r_D, respectively.
3) The shunt capacitances include MOSFET drain-to-source capacitances. The nonlinearity of the MOSFET parasitic capacitances are ignored. Additionally, the shunt capacitances at top and bottom switches are identical, namely $C_{S1j} = C_{S2j}$.
4) The equivalent series resistances (ESRs) of all components are considered. However, they are sufficient small not to affect the waveforms.
5) The switches S_{11} and S_{21} turn on at $\theta = 0$ and $\theta = \pi$, respectively, with duty ratio D. Additionally, the class-D inverters 1 and 2 are driven with phase shift ϕ.
6) The component values of the inverter 1 are the identical to those of the inverter 2.

For the circuit-equation formulations, the normalized parameters are defined as follows.

a) $\omega = 2\pi f$: The angular operating frequency.
b) $\omega_{in} = 2\pi f_{in} = 1/(\sqrt{L_r C_r})$: The resonant angular frequency of the inverter.
c) $A_{in} = (f_{in}/f) = \omega_{in}/\omega$: The ratio of resonant frequency of the inverter to operating frequency.
d) $B_{in} = C_S/C_r = (C_{S1} + C_{S2})/C_r$: The ratio of the sum of shunt capacitances of switches to resonant capacitance of the inverter.
e) $\omega_f = 2\pi f_f = 1/(\sqrt{L_f C_f})$: The cut-off angular frequency of the low-pass filter.
f) $A_{re} = (f_f/f) = \omega_f/\omega$: The ratio of cut-off frequency of the low-pass filter to operating frequency.
g) $B_{re} = C_D/C_f$: The ratio of the shunt capacitance of the rectifier diode to low-pass filter capacitance of the rectifier.
h) $H = L_r/L_f$: The ratio of resonant inductance of the inverter to low-pass filter inductance of the rectifier.
i) $Q = (\omega L_r)/R$: The parameter like loaded quality factor of the inverter.

From the above assumptions and normalized parameters, the circuit equations are

$$\begin{cases} \dfrac{d}{d\theta}\dfrac{Ri_{rj}}{V_I} = \dfrac{1}{Q}\left(\dfrac{v_{S_{1j}}}{V_I} - \dfrac{v_{C_{rj}}}{V_I} - \dfrac{v_D}{V_I} - \dfrac{r_{L_r}}{R}\cdot\dfrac{Ri_{rj}}{V_I}\right) \\ \dfrac{d}{d\theta}\dfrac{v_{C_{rj}}}{V_I} = A_{in}^2 Q\cdot\dfrac{Ri_{rj}}{V_I} \\ \dfrac{d}{d\theta}\dfrac{v_{S_{1j}}}{V_I} = \dfrac{A_{in}^2 Q}{B_{in}}\left[\left(\dfrac{R}{R_{S2j}}\right) - \left(\dfrac{R}{R_{S1j}} + \dfrac{R}{R_{S2j}}\right)\dfrac{v_{S_{1j}}}{V_I} - \dfrac{Ri_{rj}}{V_I}\right] \\ \dfrac{d}{d\theta}\dfrac{v_D}{V_I} = \dfrac{A_{re}^2 Q}{B_{re}H}\left[\dfrac{R(i_{r1}+i_{r2})}{V_I} - \dfrac{R}{R_D}\cdot\dfrac{v_D}{V_I} - \dfrac{Ri_f}{V_I}\right] \\ \dfrac{d}{d\theta}\dfrac{Ri_f}{V_I} = \dfrac{H}{Q}\left(\dfrac{v_D}{V_I} - \dfrac{v_f}{V_I} - \dfrac{r_{L_f}}{R}\cdot\dfrac{Ri_f}{V_I}\right) \\ \dfrac{d}{d\theta}\dfrac{v_f}{V_I} = \dfrac{A_{re}^2 Q}{H}\left(\dfrac{Ri_f}{V_I} - \dfrac{v_f}{V_I}\right), \quad j = 1 \text{ and } 2, \end{cases} \tag{9}$$

where R_{S1}/R, R_{S2}/R, and R_D/R are the normalized resistances of the bottom switch of the inverter 1, that of the inverter 2, and the rectifier diode, respectively. The normalized resistances of the bottom switches of the inverter are given by

$$\frac{R_{Sj}}{R} = \begin{cases} \dfrac{r_S}{R}, \text{ if } D_{rj} \text{ is in on-state,} \\ \infty, \text{ if } D_{rj} \text{ is in off-state and } \quad 0 \le \dfrac{v_{S1j}}{V_I} < 1. \\ \dfrac{r_{SD}}{R}, \text{ otherwise.} \end{cases} \tag{10}$$

Similarly, the normalized resistance of the rectifier diode is

$$\frac{R_D}{R} = \begin{cases} \dfrac{r_D}{R} & \text{for } \dfrac{v_D}{V_I} \le \dfrac{v_{th}}{V_I}, \\ \infty & \text{for } \dfrac{v_D}{V_I} > \dfrac{v_{th}}{V_I}, \end{cases} \tag{11}$$

where v_{th} is the threshold voltage of the rectifier diode. When we define $\boldsymbol{x}$ is $\boldsymbol{x} = [x_1, x_2, \cdots, x_9] = [Ri_{r1}/V_I,\ Ri_{r2}/V_I,\ v_{Cr1}/V_I,\ v_{Cr2}/V_I,\ v_{S1}/V_I,\ v_{S2}/V_I,\ v_D/V_I,\ Ri_f/V_I,\ v_f/V_I\ ]^T \in \boldsymbol{R}^9$ and $\boldsymbol{\lambda} = [Q, A_{in}, A_{re}, B_{in}, B_{re}, H, D, R, r_S/R, r_{SD}/R, r_D/R, r_{L_r}/R, r_{L_f}/R, V_I, \phi\ ]^T \in \boldsymbol{R}^{15}$, it is seen that the circuit equations in (9) corresponds to (1). The voltage and current waveforms $\boldsymbol{\varphi}$ can be obtained by applying the Runge-Kutta method to (9).

3.4. Drawing the ZVS Region

For drawing the ZVS region, it is necessary to express the boundary condition of switching states between ZVS and non-ZVS. In this paper, the switching states of the bottom switches are considered because of symmetric operations between the top and bottom switches.

Because the waveforms in the steady state are periodic orbit with 2π, the steady-state condition corresponding to (5) is

$$\boldsymbol{\varphi}(2\pi, \boldsymbol{x}_0, \boldsymbol{\lambda}) - \boldsymbol{x}_0 = \boldsymbol{0} \quad \in \boldsymbol{R}^9. \tag{12}$$

The boundary condition between ZVS and non-ZVS means that the switch-voltage waveform reaches zero from positive to negative direction at switch turn-on instant. Namely, we have

$$\varphi_5(2\pi) = 0 \text{ and } \frac{d\varphi_5(2\pi)}{d\theta} < 0 \text{ for the inverter 1} \tag{13}$$

and

$$\varphi_6(2\pi + \phi) = 0 \text{ and } \frac{d\varphi_6(2\pi + \phi)}{d\theta} < 0 \text{ for the inverter 2.} \tag{14}$$

By solving (12)-(14) successively with the curve tracking algorithm, it is possible to draw the boundary curve between the ZVS and non-ZVS regions on the parameter space. When a parameter set satisfies all of two conditions, the ZVS can be achieved at both the inverters 1 and 2.

3.5. Computation Results

The component values according to the concrete design specifications can be obtained by using the normalized parameters. In this design example, the design specifications are given as: the operating frequency $f = 400$ kHz, the load resistance $R = 50\ \Omega$, and the maximum output power $P_{omax} = 50$ W. The output power is controlled from 50 W to 0 by varying the phase shift ϕ. From $R = 50\ \Omega$ and $Q = 3$, the resonant inductance $L_r = 59.7\ \mu$H was obtained.

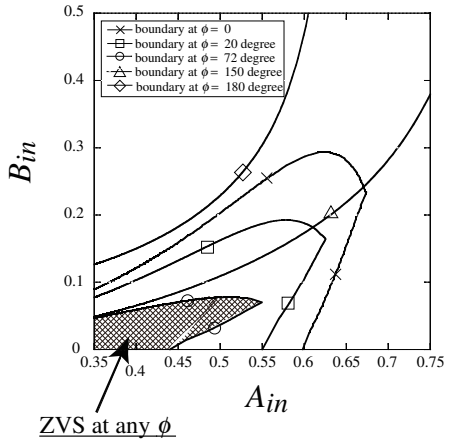

Figure 2: Boundary of ZVS or non-ZVS region for fixed phase shifts and ZVS region at any phase shifts on A_{in} and B_{in} space.

Table 1: Component Values and Characteristics of Phase-Controlled Resonant dc-dc Converter.

	Calculated	Measured	Difference
C_{r1}	9.96 nF	10.0 nF	0.53 %
C_{r2}	9.96 nF	10.0 nF	0.53 %
C_{S1}	684 pF	673 pF	-0.17 %
C_{S2}	684 pF	670 pF	-0.21 %
C_D	5.14 nF	5.14 nF	0.00 %
L_f	300 μH	303 μH	1.00 %
C_f	5.28 μF	5.28 μF	0.00 %
P_o	50.0 W	49.8 W	-0.004 %
η	95.8%	91.9%	-3.90 %

Also, $H = 0.2$, $A_{re} = 0.01, B_{re} = 0.001$, $r_D/R = 0.05$, $D_{re} = 0.5$, $r_S/R = r_{SD}/R = 0.05$ are given. Because of $H = 0.2$, the inductance of low-pass filter was L_f =300μH. The inductors of L_{r1}, L_{r2}, and L_f were made posterior to the component value derivations, and ESRs of inductances were measured as $r_{Lr1} = 0.28\ \Omega$, $r_{Lr2} = 0.27\ \Omega$, and $r_{Lf} = 0.11\ \Omega$. The input voltage for achieving 50 W output power for $\phi = 0$ is $V_I = 116$ V. Figure 2 shows the superimposed boundary curves for the fixed phase shift. The narrowest ZVS region appears at $\phi = 72°$ in this design example. Additionally, it can be confirmed from Fig. 2 that the ZVS region for $\phi = 72°$ covers with the ZVS regions at other phase shifts. Namely, the converter, which achieves the ZVS at any phase shifts, can be designed by selecting a set of parameters A_{in} and B_{in} from the dotted region in Fig. 2, which is the ZVS region for $\phi = 72°$. In this design example, we selected the parameter set of $A_{in} = 0.51$ and $B_{in} = 0.068$. By using this parameter set, it is possible to achieve the ZVS at any phase shifts with high output power.

3.6. Experimental Verifications

Circuit experiments and PSpice simulations were carried out for showing the validity of the converter design. Table 1 gives the component values.

Figure 3 shows superimposed waveforms of numerical calculations, PSpice simulations, and experimental measurements for $\phi = 72°$. The ZVS region is the narrowest at $\phi = 72°$. It was confirmed from Fig. 3 that both inverters 1 and 2 achieved the ZVS at $\phi = 72°$. Namely, the phase-controlled resonant converter with class-D ZVS inverter could be designed successfully. This result showed the validity of the ZVS-region map as shown in Fig. 2. Additionally, the numerical waveforms agreed with the experimental and PSpice simulation waveforms quantitatively, which showed the validity of circuit-model formulations and the steady-state waveform derivations.

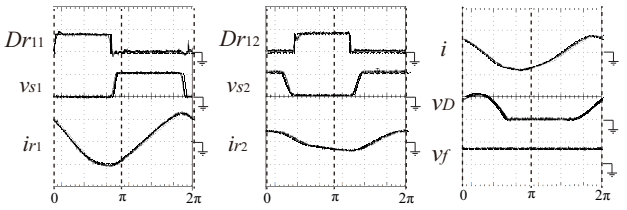

Figure 3: Waveforms of numerical calculations (dashed line) ,PSpice simulations (dotted line) and circuit experiments (solid line) for $\phi = 72°$. Vertical : D_{r11}, D_{r12}:10 V/div, v_{S11}, v_{S12}:100 V/div, i_{r1}, i_{r2}:1 A/div, i:2 A/div, v_D:200 V/div, v_f:50 V/div and Horizontal : 400 ns/div in PSpice simulations and circuit experiments.

4. Conclusion

This paper has been proposed design method of resonant converters applying computation algorithm of bifurcation values. As a design example, the phase-controlled resonant dc-dc converter with the class-D ZVS inverter and the class-E rectifier is designed. It is possible forth designed converter to achieve the ZVS condition at any phase shifts. The validity of the design method was confirmed from the quantitative agreements with PSpice-simulation and experimental results.

References

[1] C. Ji, P. Zanchetta, F. Carastro, and J. Clare, "Repetitive control for high-performance resonant pulsed power supply in radio frequency applications," *IEEE Trans. Ind. App.*, vol. 50, no. 4, pp. 2660 – 2670, Jul. 2014.

[2] M. Pinuela, D. C. Yates, S. Lucyszyn, and P. Mitcheson, "Maximizing DC to load efficiency for inductive power transfer," *IEEE Trans. Power Electron.*, vol. 28, no. 5, pp. 2437–2447, May. 2013.

[3] G. Yadav and N. Narasamma, "An active soft switched phase-shifted full-bridge dc-dc converter: analysis, modeling, design, and implementation," *IEEE Trans. Power Electron.*, vol. 29, no. 9, pp. 4538–4550, Sept. 2014.

[4] H. Kawakami, "Bifurcation of periodic responses in forced dynamic nonlinear circuits: Computation of bifurcation values of the system parameters," *IEEE Trans. Circuits Syst.*, vol. CAS-31, pp. 248–260, Apr. 1984.